14th International Symposium on Turbulence and Shear Flow Phenomena (TSFP14)
Heidelberg, Germany, July 28–31, 2026

WAVEPACKET APPROXIMATIONS TO RESOLVENT ANALYSIS FOR WALL-BOUNDED PARALLEL SHEAR FLOWS

Barbara Lopez-Doriga
Mechanical and Aerospace Engineering
University of California, Los Angeles
Los Angeles, California, 90095 USA
bldoriga@ucla.edu

Scott T. M. Dawson
Mechanical, Materials, and Aerospace Engineering Department
Illinois Institute of Technology
Chicago, Illinois, 60616 USA
sdawson5@illinoistech.edu

ABSTRACT

This work develops an approach for approximating the properties of the pseudospectra (or equivalently, performing resolvent analysis) of linear operators related to wall-bounded shear flows. This provides a means for predicting the properties of energetically-dominant coherent structures at specific length- and time-scales. The method assumes that leading resolvent modes (i.e., pseudoeigenmodes) of a given linear operator can be expressed as a sum of wavepackets with a given template shape, and then recasts the associated optimization problem as the minimization of a cost function over a low-dimensional space of parameters. In some cases, this global cost function can be explicitly computed, while for more complex cases the cost function can be optimized using iterative gradient descent methods, requiring only local function evaluations. We demonstrate that this methodology can be used to identify both optimal and suboptimal mode shapes, and that the use of image modes allows this method to be applied to wall-attached modes, where the mode shape is influenced by the presence of boundaries. We further show that the wavepacket method is able to capture the correct symmetry or antisymmetry of leading resolvent modes in cases where multiple critical layers are present sufficiently close to each other to allow interaction between the corresponding mode structures in their vicinity.

INTRODUCTION

The analysis of linearized operators has a lengthy history in the context of studying the stability and emergent structures within several classes of inviscid (Rayleigh, 1880; Tollmien, 1936; Fjørtoft, 1950) and viscous (Drazin & Reid, 2004; Lin, 1956) flow. For parallel shear flows, the asymptotic stability of the linearized Navier–Stokes equations does not typically concur with observations. For example, Couette and pipe flows are linearly asymptotically stable for all Reynolds numbers (proven analytically for the Couette case by (Romanov, 1973)), while for planar channel flow, transition to turbulence occurs at much lower Reynolds numbers than the critical Reynolds number predicted by asymptotic stability (around 5772, as first accurately computed by Orszag (Orszag, 1971)). However, beyond looking at eigenvalues, linear analyses can still provide substantial insight into the dynamics of such flows. In particular, parallel shear flows are typically associated with highly nonnormal linearized operators, which can give rise to large transient energy growth and amplification of disturbances, even when the operators are asymptotically stable (Böberg & Brösa, 1988; Trefethen *et al.*, 1993; Schmid & Henningson, 2012).

Here, we focus on resolvent analysis (McKeon & Sharma, 2010), which identifies the coherent structures that are most highly amplified by the mean-linearized equations at specified length and timescales. Equivalently, this method identifies pseudoeigenvectors corresponding to spatial structures that are the closest to being eigenvectors of the linearized equations for a given frequency. For nonnormal operators in particular, it is possible to have structures that are close to being eigenvectors (in the sense that they are highly amplified by the linear dynamics) even when the specified frequency is not near an eigenvalue (Trefethen *et al.*, 1993; Trefethen & Embree, 2005).

Most typically, resolvent analysis proceeds by numerically computing the (truncated) singular value decomposition (SVD) of a linear operator, either from explicit matrix-forming or implicitly using timestepping methods (Martini *et al.*, 2021; Farghadan *et al.*, 2025). Here, we propose an alternative formulation that assumes that resolvent modes can be approximated by functions of a prescribed form. The approach that we use is inspired by the findings of Trefethen & Chapman (2004); Trefethen (2005), who identified the conditions under which the pseudoeigenmodes of certain matrices and linear operators corresponding to large energy amplification are localized both in both space and spatial frequency, and thus can be represented by wavepackets possessing these properties. This theory has been previously applied in the context of flow near the attachment line of a swept body (Obrist & Schmid, 2010, 2011), a Batchelor vortex (Mao & Sherwin, 2011), and a wingtip vortex in an airfoil wake (Edstrand *et al.*, 2018). This wavepacket pseudomode theory also has connections with classical Wentzel-Kramers-Brillouin-Jeffreys theory (Wentzel, 1926; Kramers, 1926; Brillouin, 1926; Jeffreys, 1925), which has been applied in the context of modeling wall-bounded turbulent flows in (Leonard, 2016).

Exploiting this theory, previous work has developed a method to approximate resolvent mode shapes using analytic functions, which is valid for detached modes which are localized about a critical layer (Dawson & McKeon, 2019). These ideas have subsequently been applied to predict mode shape components for supersonic flows (Dawson & McKeon, 2020), and for the analysis of amplitude modulation through consideration of Reynolds stress modes (Jacobi *et al.*, 2021).

In the present work, we extend this analysis to more complex mode shapes, that account for the effects of boundary conditions, multiple critical layers, and suboptimal modes. This requires the use of a more general assumed mode shape, where instead of using a single wavepacket we instead assume that the mode can be approximated by a sum of such wavepackets of the form

$$\psi_a(y) = \sum_{j=1}^{r} C_j \exp\left[ik_{y,j}(y-y_{0,j}) - q_{y,j}(y-y_{0,j})^2\right] \quad (1)$$

for a suitably-chosen value of r, where $k_{y,j}, q_{y,j}, y_{0,j}$ and C_j are parameters to be determined, and the c_j's are scaled to ensure the function has unit norm. Here and henceforth, the subscript a indicates that we are using this wavepacket approximation to a resolvent mode.

METHODOLOGY

Our analysis will focus on incompressible parallel shear flow, formulated in wall-normal velocity ($\hat{v}$) and vorticity ($\hat{\eta}$) coordinates. The resolvent form of these equations can be expressed as (Rosenberg & McKeon, 2019)

$$\begin{pmatrix}\hat{v}\\ \hat{\eta}\end{pmatrix} = \underbrace{\begin{pmatrix}\mathcal{H}_{OS} & 0\\ ik_z\mathcal{H}_{SQ}U_y\mathcal{H}_{OS} & \mathcal{H}_{SQ}\end{pmatrix}}_{\mathcal{H}} \begin{pmatrix}\hat{f}_v\\ \hat{f}_\eta\end{pmatrix} \quad (2)$$

$$\mathcal{H}_{OS} = \left(-i\omega + \Delta^{-1}\left[ik_xU\Delta - ik_xU_{yy} - \frac{1}{Re}\Delta^2\right]\right)^{-1} \quad (3)$$

$$\mathcal{H}_{SQ} = \left(-i\omega + ik_xU - \frac{1}{Re}\Delta\right)^{-1} \quad (4)$$

where $\mathcal{H}$ is the resolvent operator of the full system and $\mathcal{H}_{OS}$ and $\mathcal{H}_{SQ}$ are the resolvents associated only with the Orr-Sommerfeld and Squire operators. In this formulation, ω, k_x and k_z denote the temporal frequency and streamwise and spanwise wavenumbers, $\Delta = \partial_{yy} - k_x^2 - k_z^2$ is the Laplacian operator, and U, U_y and U_{yy} are the mean streamwise velocity and its first and second derivatives in the wall-normal direction. Resolvent analysis proceeds by considering the SVD $\mathcal{H} = \sum_{j=1}^{n}\psi_j\sigma_j\phi_j^* \approx \sum_{j=1}^{q\ll n}\psi_j\sigma_j\phi_j^*$ where the left and right singular vectors ψ_j and ϕ_j are to response and forcing modes respectively, with the leading modes corresponding to the largest energy amplification by the linearized dynamics. These leading singular value and vectors of the resolvent operator also satisfy a set of associated optimization problems, including

$$\psi_1 = \underset{\psi:\ \|\psi\|=1}{\operatorname{argmax}}\ \|\mathcal{H}^*\psi\| = \underset{\psi:\|\psi\|=1}{\operatorname{argmin}}\ \|\mathcal{H}^{-1}\psi\| \quad (5)$$

meaning in particular that pseudospectral (resolvent) analysis can be equivalently formulated as an optimization problem. If we assume that the resolvent response mode takes the form given in equation 1, then equation 5 becomes an optimization problem that can be expressed as

$$\{\boldsymbol{C}, \boldsymbol{k}, \boldsymbol{q}, \boldsymbol{y}_0\} = \underset{\mathbf{c},\boldsymbol{k},\boldsymbol{q},\boldsymbol{y}_0}{\operatorname{argmin}} \left\|\mathcal{H}^{-1}\psi_a\right\|^2 \quad (6)$$

where the set of vectors $\{\mathbf{c}, \boldsymbol{k}, \boldsymbol{q}, \boldsymbol{y}_0\}$ includes all of the parameters required to define equation 1. Assuming that only a small number of wavepackets are needed, this optimization problem in equation 6 is typically much lower dimensional than that associated with the SVD, though it is now nonlinear. Depending on the number of wavepackets used and the form of the resolvent operator under consideration, the cost function

$$\mathcal{J} = \left\|\mathcal{H}^{-1}\psi_a\right\|^2 \quad (7)$$

and its derivatives can either be computed globally in closed form, or can be evaluated locally as needed to perform gradient descent based optimization. For the purposes of this work, we will focus exclusively on the shape of the $\hat{\eta}$ component of the response mode, which typically has a much larger contribution to the energy than the $\hat{v}$ component. To ensure that the wavepacket modes given by equation 1 satisfy the appropriate no-slip boundary conditions, we utilize appropriately constructed image wavepackets. To determine the total number of wavepackets required for a given mode, we assume that the critical layer mechanism drives amplification, where the critical layer is the location y_c at which the wavespeed $c = \omega/k_x = U(y_c)$. From this we utilize the following rules:

1. The leading mode contains one wavepacket within the domain for each critical layer (e.g., one for Couette flow, two for Poiseuille flow), while suboptimal modes use an additional wavepacket within the domain at each critical layer.
2. An equal number of image wavepackets are introduced for each boundary that a wavepacket is "attached" to.

A schematic showing how these wavepackets are combined in various cases is illustrated in figure 1.

We now provide some explicit examples that will be used in the following analysis. The template for a mode that has a single wavepacket within the domain and a corresponding image wavepacket to enforce boundary conditions at $y = y_b$ (configuration depicted in figure 1(e)) has the form

$$\begin{aligned}\psi_\eta(y) =& C_1\left\{\exp\left[ik_y(y-y_0) - q_y(y-y_0)^2\right]\right.\\ &\left.-\exp\left[-ik_y(y+y_0-2y_b) - q_y(y+y_0-2y_b)^2\right]\right\}\end{aligned} \quad (8)$$

For cases with a base or mean flow that is symmetric about $y = 0$, there can be critical layers located on either side of the plane of symmetry, and modes that are sufficiently far away from the boundary (configurations depicted in figure 1(c-d)) can be represented by

$$\begin{aligned}\psi_\eta(y) =& C_1\left\{\exp\left[ik_y(y-y_0) - q_y(y-y_0)^2\right]\right.\\ &\left.\pm\exp\left[-ik_y(y+y_0) - q_y(y+y_0)^2\right]\right\}\end{aligned} \quad (9)$$

where the $+$ and $-$ in front of the second term yield modes that respectively symmetric and antisymmetric about the midplane. When the two wavepackets in equation (9) are sufficiently sep-

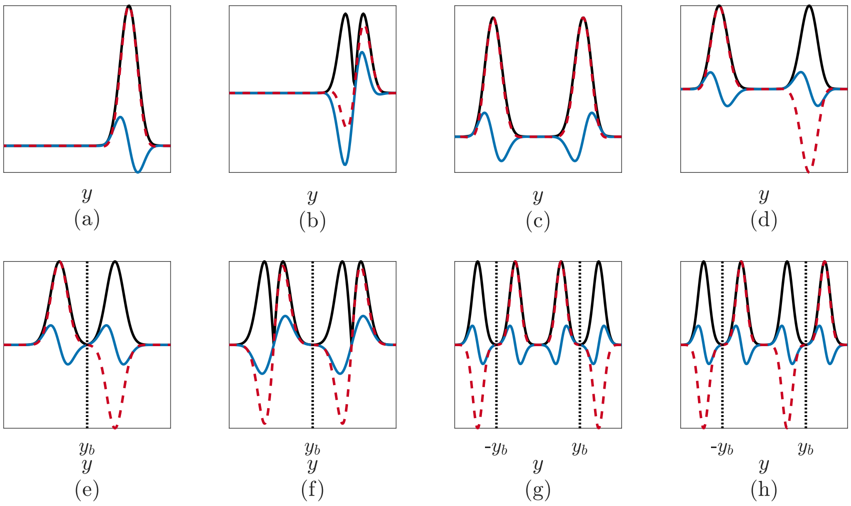

Figure 1: Real (red), imaginary (blue) and absolute (black) components of the numerically computed (a-d) and analytic approximations (e-h) of the optimal and suboptimal resolvent modes of $\mathcal{H}_{\eta\eta,\boldsymbol{\omega}}$ for Couette (first and second columns) and Poiseuille (third and fourth columns) flows contained in the domain $-y_b \leq y \leq y_b$ with $y_b > 0$.

arated, the symmetric and antisymmetric cases have the same amplification, but when they overlap this is not the case.

In equations (8)-(9), the parameters to optimize over in equation 6 are $\{k_y, q_y, y_0\}$, with C_1 set such that the mode has unit norm when integrated over the physical domain (which often excludes much of any image wavepacket).

RESULTS

Results from two different broad cases will be shown. First, we will show results where we consider only the Squire component ($\mathcal{H}_{SQ}$) of equation 2 for laminar plane Poiseuille flow, which is sufficiently simple that the global cost function $\mathcal{J} = \left\| \mathcal{H}_{SQ}{}^{-1} \psi_a \right\|^2$ can be computed in closed form. Following this, we consider the full system, and optimize the cost function by local numerical evaluations.

Wavepacket approximations for the Squire equation

We first show results applying this methodology to approximate resolvent modes of the Squire operator $\mathcal{H}_{SQ}$ for laminar plane Poiseuille flow at a Reynolds number of 3000, with a mean velocity given by $U(y) = 1 - y^2$. In this case, the cost function corresponding to equation 7 can be explicitly evaluated. For example, letting $R = k_x Re$, a wavepacket-based mode with the form given by equation 10 gives

$$\mathcal{J} = -\frac{k_x^2}{k_x^2 + k_z^2} \left[J_1 - q_y^2 e^{\frac{k_y^2}{2q_y} + 2q_y y_0^2} J_2 \right] J_3 \qquad (10)$$

$$\begin{aligned} J_1 =& a^4 R^2 - 128 k_y q_y^4 R y_0 y_c + 128 q_y^5 \omega_i R (1 - 4 q_y y_0^2) y_c^2 + \\ & 64 q_y^6 [3 + 8 q_y y_0^2 (-3 + 2 q_y y_0^2)) y_c^2 + 2 k_y^2 b R^2 (-3 + 4 q_y y_c^2) \\ & + q_y^2 R^2 (3 + 8 q_y y_c^2 (-1 + 2 q_y (4 \omega_i^2 + y_c^2))] \end{aligned}$$

$$\begin{aligned} J_2 =& 64 q_y^2 (k_y^4 + 6 k_y^2 q_y + 3 q_y^2) y_c^2 + \\ & 128 q_y^2 R y_c [-k_y y_0 + (k_y^2 + q_y) \omega_i y_c] + R^2 [3 + \\ & 8 q_y (2 q_y y_0^4 + y_0^2 (3 - 4 q_y y_c^2) + y_c^2 (-1 + 8 q_y \omega_i^2 + 2 q_y y_c^2))] \end{aligned}$$

$$J_3 = \left[64 q_y^4 R^2 y_c^2 \left(-1 + e^{\frac{k_y^2}{2q_y} + 2 q_y y_0^2} \right) \right]^{-1}$$

Figure 2 shows the leading resolvent mode amplitude and phase variation across a portion of the channel, for various complex frequencies $\omega = \omega_r + i\omega_i$, and various numbers of wavepackets. Subplots (a,e) shows that when the critical layer is close to the wall, including image wavepackets on the opposite side of the wall can accurately capture the shape of wall-attached modes. When the critical layer is further from the wall as in subplots (b,f), a single wavepacket is sufficient to capture the mode shape about one of the two critical layers within the domain (with the second not shown in the plots). When the critical layer is in the center of the domain as in subplots (c,d,g,h), having two wavepackets within the domain is sufficient for capturing the mode shape for both the leading and secondary resolvent mode.

Figure 3 shows that these wavepacket-based approximation methods can also accurately capture the singular values associated with the leading and second (suboptimal) modes. Departures from the true amplification levels occur for small ω_r (corresponding to critical layers near the walls) in the absence of image wavepackets to enforce boundary conditions (the red dotted curves), and for large ω_r if only using a single wavepacket within the domain (blue dashed curves).

Wavepacket approximations for the linearized Navier-Stokes equations

We now consider approximation of the leading resolvent modes of the full system given by equation 2. In this equation, it is often the off-diagonal block mapping forcing in $\hat{v}$ to response in $\hat{\eta}$ that is primarily responsible for leading amplification mechanisms, so we will focus on approximating the leading singular values and vectors of this sub-operator, given by

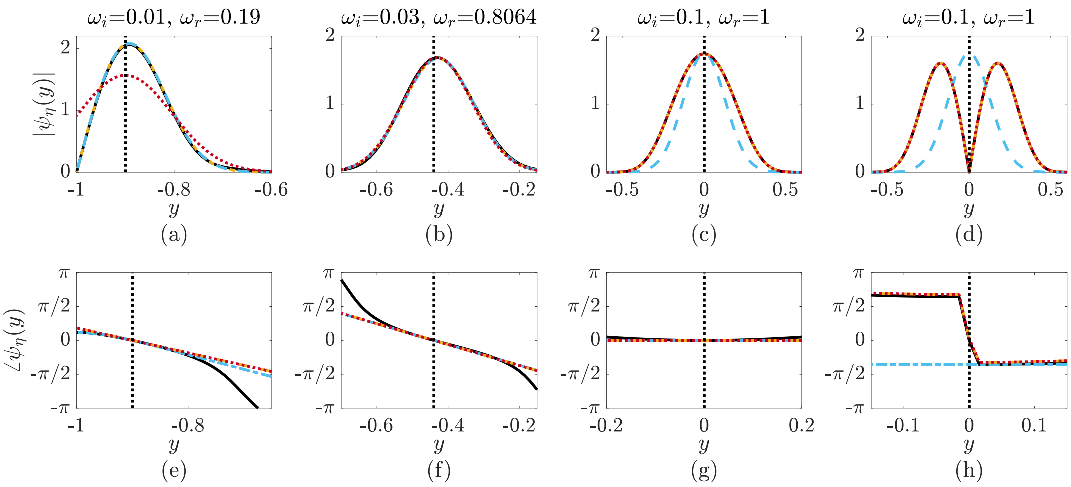

Figure 2: Prediction of the magnitude $|\psi_\eta|$ and phase variance $\angle\psi_\eta$ using a single wavepacket with an image wavepacket to enforce boundary conditions (blue) two wavepackets within the domain with (yellow) and without (red) image wavepackets, for the Squire operator associated with plane Poiseuille flow at $Re = 3000$. The black curves show the numerical solutions, while the dotted vertical lines indicate critical layer locations where $U(y) = c_r = \omega_r/k_x$. Subplots (a-c,e-g) show leading modes for various complex frequencies $\omega = \omega_r + i\omega_i$, while subplots (d,h) show the secondary mode with the same ω values as subplots (c,g).

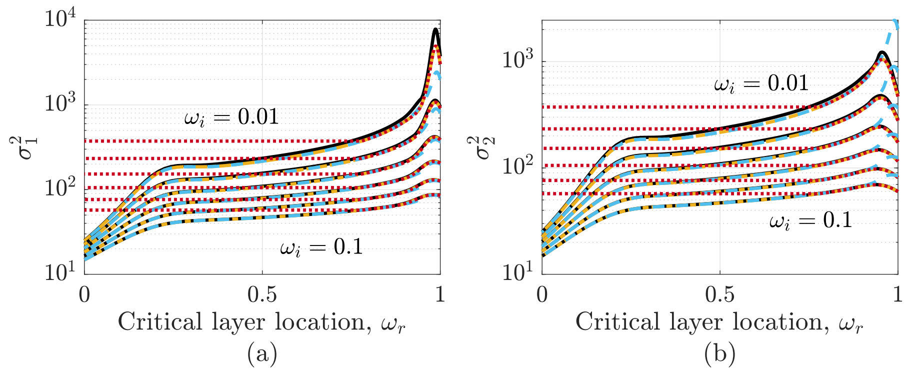

Figure 3: Prediction of the (a) optimal and (b) suboptimal mode amplification levels for the Squire operator for Poiseuille flow at $Re = 3000$. Black curves show the true (numerical) solution, while the colored curves show predictions with various numbers of wavepackets, as indicated in the caption of figure 2. Note that red curves do not account for boundary conditions, whereas blue and yellow curves do.

$$\mathcal{H}_{v\eta} = ik_z\mathcal{H}_{SQ}U_y\mathcal{H}_{OS}. \tag{11}$$

In this case, rather than finding an explicit global expression for the cost function, we find the wavepacket parameters through numerical optimization of equation 6. We consider turbulent channel flow at a friction Reynolds number $Re_\tau = 2000$, with a mean profile computed using an eddy viscosity model Reynolds & Tiederman (1967).

We first consider wavenumbers $(k_x, k_z) = (4\pi, 40\pi)$, matching those considered e.g. in Symon *et al.* (2018) as representative of the near-wall cycle (NWC). Figure 4 shows the amplification of the leading mode of the full operator, alongside that of $\mathcal{H}_{v\eta}$, and an approximation to the latter obtained using equation 8. We observe that $\mathcal{H}_{v\eta}$ has similar leading singular values to the full operator $\mathcal{H}$ across most frequencies, with the discrepancy growing with wavespeed. However, the wavepacket approximation of the leading modes of $\mathcal{H}_{v\eta}$ gives singular values that closely match the numerically-computed values. In other words, the main discrepancy between the gain of the full operator and the analytic approximation comes from the simplification of only considering $\mathcal{H}_{v\eta}$, rather than the restriction of the modes to have the appropriate wavepacket form. Figure 5 compares the shape of the numerically computed modes, and wavepacket approximation, where close agreement is found across all selected wavespeeds. In particular, the wavepacket approximation is able to capture the differences between the mode peak and critical layer location due to the presence of the wall.

We next consider wavenumbers $(k_x, k_z) = (\pi/9, 2\pi/3)$, corresponding to lengthscales representative of very large scale motions (VLSM), again matching the considered in Symon *et al.* (2018). The resolvent gains for this case across a range of wavespeeds are shown in figure 6. In this case, we consider

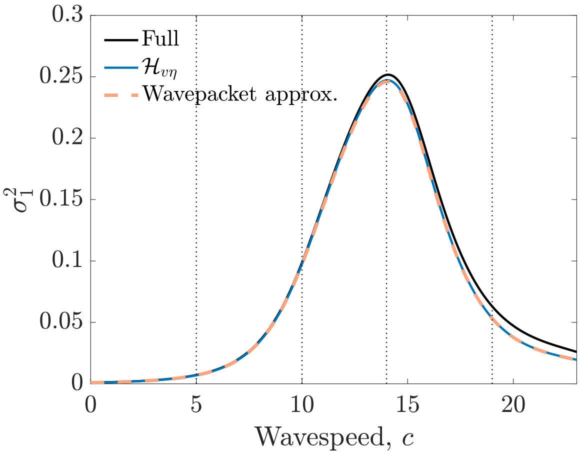

Figure 4: Resolvent gain for NWC parameters, computed numerically and using wavepacket approximations. Vertical lines indicates wavespeeds for which corresponding modes are compared in figure 5.

wavepacket approximations given by both a single wavepacket, and using two wavepackets as given in equation (9). In the region of large amplification, we observe regions where both the symmetric and antisymmetric pairs of wavepackets give the closest approximation to the true resolvent gain. Figure 7 we compare the numerically computed resolvent modes to the wavepacket approximation corresponding to largest gain. It is observed that the wavepacket method can correctly predict the region where the symmetric and antisymmetric modes yield the largest gain. The wavepacket approximations also very closely predict the shape of the numerically computed modes, with the largest discrepancy being observed near the center of the domain in the antisymmetric case. Note that unlike the NWC case, the use of two wavepackets within the domain is necessary to obtain an accurate estimation of the properties of the leading modes.

CONCLUSIONS

This work has introduced a method for approximating leading resolvent amplification mechanisms using wavepackets of a prescribed form. The method does not require knowledge of the true solution, but rather infers an approximation to the linear amplification properties of the resolvent via an optimization problem over the wavepacket parameters, which is directly analogous to the optimization problem corresponding to the SVD of the resolvent.

The wavepacket-based optimization problem can be solved through several approaches. In cases where the underlying operator is sufficiently simplified, such as when considering the Squire operator rather that the full linearized Navier-Stokes system with a linear or parabolic base flow, the cost function for optimizing wavepacket parameters can be found globally in closed form. For more complex cases, the optimization problem (which remains over a small number of parameters) can be solved using iterative numerical methods such as gradient descent.

It has been demonstrated that using modes consisting of multiple wavepackets can captures behavior that a single wavepacket cannot. This includes the exact matching of boundary conditions through the use of image wavepackets, and the use of symmetric and antisymmetric wavepackets across a plane of geometrical symmetry.

The analysis considered here relied upon an initial simplification of the equations to focus on a single amplification mechanism. Further work could combine this approach with methods to detect dominant amplification mechanisms automatically (Dawson *et al.*, 2025), and investigate its applicability to extensions of resolvent analysis, such as sparsity-promoting variants (Skene *et al.*, 2022; Lopez-Doriga *et al.*, 2024) that would alter optimal mode shape parameters through modification of the underlying cost function. Beyond this, the largest practical benefit of these wavepacket approaches would likely involve more complex flows with multiple spatio-temporal dimensions of inhomogeneity, for which conventional approaches require the numerical decomposition (either explicitly or implicitly) of high-dimensional operators.

ACKNOWLEDGMENTS

This work is supported by the US National Science Foundation award CBET-2238770 and US Department of Energy award DE-SC0025597.

REFERENCES

Böberg, L. & Brösa, U. 1988 Onset of turbulence in a pipe. *Zeitschrift für Naturforschung A* **43** (8-9), 697–726.

Brillouin, L. 1926 La mécanique ondulatoire de Schrödinger; une méthode générale de résolution par approximations successives. *CR Acad. Sci* **183** (11), 24–26.

Dawson, S. T. M. & McKeon, B. J. 2019 On the shape of resolvent modes in wall-bounded turbulence. *Journal of Fluid Mechanics* **877**, 682–716.

Dawson, S. T. M. & McKeon, B. J. 2020 Prediction of resolvent mode shapes in supersonic turbulent boundary layers. *International Journal of Heat and Fluid Flow* **85**, 108677.

Dawson, S. T. M., Prado Zayas, J & Lopez-Doriga, B. 2025 Sparsity-promoting methods for isolating dominant linear amplification mechanisms in wall-bounded flows. *International Journal of Heat and Fluid Flow* **115**, 109872.

Drazin, P. G. & Reid, W. H. 2004 *Hydrodynamic Stability*. Cambridge University Press.

Edstrand, A. M., Schmid, P. J., Taira, K. & Cattafesta, L. N. 2018 A parallel stability analysis of a trailing vortex wake. *Journal of Fluid Mechanics* **837**, 858–895.

Farghadan, A., Martini, E. & Towne, A. 2025 Scalable resolvent analysis for three-dimensional flows. *Journal of Computational Physics* **524**, 113695.

Fjørtoft, R 1950 Application of integral theorems in deriving criteria of stability for laminar flows and for the baroclinic circular vortex. *Geofys* **17**, 1–52.

Jacobi, I., Chung, D., Duvvuri, S. & McKeon, B. J. 2021 Interactions between scales in wall turbulence: phase relationships, amplitude modulation and the importance of critical layers. *Journal of Fluid Mechanics* **914**.

Jeffreys, H. 1925 On certain approximate solutions of lineae differential equations of the second order. *Proceedings of the London Mathematical Society* **2** (1), 428–436.

Kramers, H. A. 1926 Wellenmechanik und halbzahlige quantisierung. *Zeitschrift für Physik* **39** (10-11), 828–840.

Leonard, A. 2016 Approximate solutions to the linearized Navier–Stokes equations for incompressible channel flow. In *Proceedings of the 20th Australasian Fluid Mechanics Conference*.

Lin, C. C. 1956 The theory of hydrodynamic stability. *Journal of Fluid Mechanics* **1**, 349 – 352.

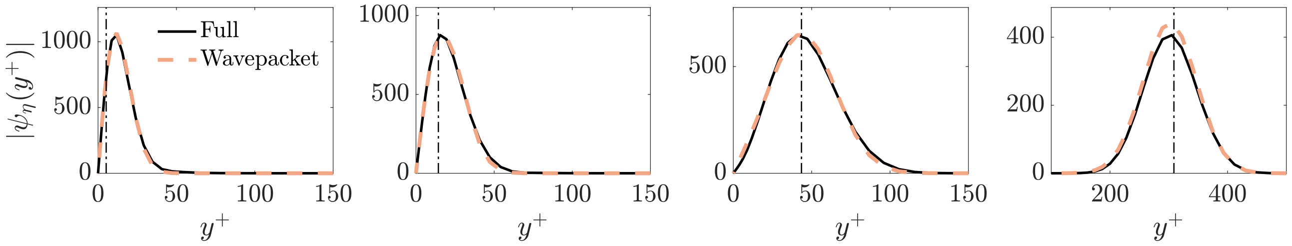

Figure 5: Full (numerically computed) and wavepacket-approximated mode shapes for NWC modes, at wavespeeds indicated by vertical lines in figure 4.

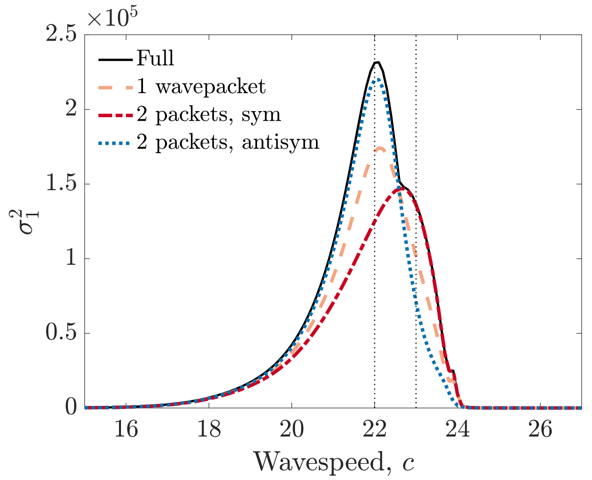

Figure 6: Resolvent gain for VLSM parameters, computed numerically and using symmetric and antisymmetric wavepacket approximations given by equation 9. Vertical lines indicates wavespeeds for which corresponding modes are compared in figure 7.

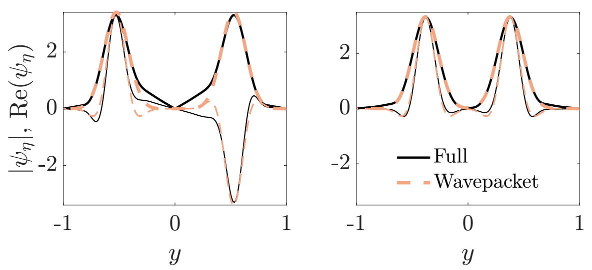

Figure 7: Full (numerically-computed) and wavepacket-approximated mode shapes for VLSM modes, at wavespeeds indicated by vertical lines in figure 6. Thick and thin lines correspond to mode amplitude ($|\psi_\eta|$) and real component (Re(ψ_η)), respectively.

Lopez-Doriga, B., Ballouz, E., Bae, H. J. & Dawson, S. T. M. 2024 Sparse space–time resolvent analysis for statistically stationary and time-varying flows. *Journal of Fluid Mechanics* **999**, A87.

Mao, X. & Sherwin, S. J. 2011 Continuous spectra of the Batchelor vortex. *Journal of Fluid Mechanics* **681**, 1–23.

Martini, E., Rodríguez, D., Towne, A. & Cavalieri, A. V. G. 2021 Efficient computation of global resolvent modes. *Journal of Fluid Mechanics* **919**.

McKeon, B. J. & Sharma, A. S. 2010 A critical-layer framework for turbulent pipe flow. *Journal of Fluid Mechanics* **658**, 336–382.

Obrist, D. & Schmid, P. J. 2010 Algebraically decaying modes and wave packet pseudo-modes in swept Hiemenz flow. *Journal of Fluid Mechanics* **643**, 309–332.

Obrist, D. & Schmid, P. J. 2011 Algebraically diverging modes upstream of a swept bluff body. *Journal of Fluid Mechanics* **683**, 346–356.

Orszag, S. A 1971 Accurate solution of the Orr–Sommerfeld stability equation. *Journal of Fluid Mechanics* **50** (04), 689–703.

Rayleigh, L. 1880 On the stability or instability of certain fluid motions. *Proc. Lond. Maths. Soc.* (11), 57–70.

Reynolds, W. C. & Tiederman, W. G. 1967 Stability of turbulent channel flow, with application to Malkus's theory. *Journal of Fluid Mechanics* **27** (2), 253–272.

Romanov, V. A. 1973 Stability of plane-parallel Couette flow. *Functional analysis and its applications* **7** (2), 137–146.

Rosenberg, K. & McKeon, B. J. 2019 Efficient representation of exact coherent states of the Navier–Stokes equations using resolvent analysis. *Fluid Dynamics Research* **51**, 011401.

Schmid, P. J. & Henningson, D. S. 2012 *Stability and transition in shear flows*. Springer Science & Business Media.

Skene, C. S., Yeh, C.-A., Schmid, P. J. & Taira, K. 2022 Sparsifying the resolvent forcing mode via gradient-based optimisation. *Journal of Fluid Mechanics* **944**.

Symon, S., Rosenberg, K., Dawson, S. T. M. & McKeon, B. J. 2018 Non-normality and classification of amplification mechanisms in stability and resolvent analysis. *Physical Review Fluids* **3** (5), 053902.

Tollmien, W 1936 General instability criterion of laminar velocity disturbances. *Nachr. Wiss fachgruppe, Gottingen, math. Phys* **1** (NACA TM-792), 79–114.

Trefethen, L. N. 2005 Wave packet pseudomodes of variable coefficient differential operators. In *Proceedings of the Royal Society of London A: Mathematical, Physical and Engineering Sciences*, , vol. 461, pp. 3099–3122. The Royal Society.

Trefethen, L. N. & Chapman, S. J. 2004 Wave packet pseudomodes of twisted Toeplitz matrices. *Communications on Pure and Applied Mathematics: A Journal Issued by the Courant Institute of Mathematical Sciences* **57** (9), 1233–1264.

Trefethen, L. N. & Embree, M. 2005 *Spectra and pseudospectra: the behavior of nonnormal matrices and operators*. Princeton University Press.

Trefethen, L. N., Trefethen, A. E., Reddy, S. C. & Driscoll, T. A. 1993 Hydrodynamic stability without eigenvalues. *Science* **261** (5121), 578–584.

Wentzel, G. 1926 Eine verallgemeinerung der quantenbedingungen für die zwecke der wellenmechanik. *Zeitschrift für Physik* **38** (6-7), 518–529.